



# Single-Atom Pd<sub>1</sub>/graphene Catalyst Achieved by Atomic Layer Deposition: Remarkable Performance in Selective Hydrogenation of 1,3-Butadiene

Huan Yan,<sup>†</sup> Hao Cheng,<sup>†</sup> Hong Yi,<sup>†</sup> Yue Lin, Tao Yao, Chunlei Wang, Junjie Li, Shiqiang Wei,<sup>\*</sup> and Junling Lu<sup>\*</sup>

Department of Chemical Physics, National Synchrotron Radiation Laboratory, Collaborative Innovation Center of Chemistry for Energy Materials (iChem), Hefei National Laboratory for Physical Sciences at the Microscale, CAS Key Laboratory of Materials for Energy Conversion, University of Science and Technology of China, Hefei, Anhui 230026 (P. R. China)

## Supporting Information

**ABSTRACT:** We reported that atomically dispersed Pd on graphene can be fabricated using atomic layer deposition technique. Aberration-corrected high-angle annular dark-field scanning transmission electron microscopy and X-ray absorption fine structure spectroscopy both confirmed that isolated Pd single atoms dominantly exist on the graphene support. In selective hydrogenation of 1,3-butadiene, the single-atom Pd<sub>1</sub>/graphene catalyst showed about 100% butenes selectivity at 95% conversion at a mild reaction condition of about 50 °C, which is likely due to the changes of 1,3-butadiene adsorption mode and enhanced steric effect on the isolated Pd atoms. More importantly, excellent durability against deactivation via either aggregation of metal atoms or carbonaceous deposits during a total 100 h of reaction time on stream was achieved. Therefore, the single-atom catalysts may open up more opportunities to optimize the activity, selectivity, and durability in selective hydrogenation reactions.

Atomically dispersed noble metal catalyst has attracted rapidly increasing attention due to its unique catalytic properties and maximized atom efficiency for low-cost.<sup>1-8</sup> However, synthesis of such single-atom catalyst (SAC) is not trivial, because metal single atoms are often very mobile on surface and tend to aggregate to form clusters or nanoparticles due to high surface free energy, especially under reaction conditions.<sup>2, 4, 9-10</sup> Synthesis of SACs from gas phase could be an even greater challenge, since it is usually carried out at elevated temperatures, which would significantly accelerate metal atom aggregations during synthesis. Indeed, Sun et al., observed the formation of a mixture of atoms, clusters and nanoparticles of Pt on graphene using atomic layer deposition (ALD),<sup>11</sup> a thin film growth technique through self-limiting binary reactions between gaseous precursors and the substrate.<sup>12-13</sup> Botton et al., also reported the formation of a mixture of Pt atoms and clusters on the N-doped graphene support using Pt ALD.<sup>14</sup>

Selective hydrogenation of 1,3-butadiene in an excess of alkenes is an important industrial process to purify the alkenes streams from petroleum cracking.<sup>15</sup> The critical requirements in this process are: (i) to achieve high selectivity to butenes, especially to 1-butene (the most desirable product) at high conversions; (ii) to minimize hydrogenation of the alkenes streams at high conversions; (iii) to achieve long durability against deactivation via carbonaceous deposits formation.<sup>16</sup> Pd-based catalysts are often used due to its high hydrogenation activity, while the selectivity to butenes, especially to 1-butene at high conversions is still poor.<sup>17-20</sup> Moreover, the gradual catalyst deactivation with time via the formation of carbonaceous deposits on catalyst surface remains as an insuperable issue, by showing a short catalyst lifetime of just a few hours or even less.<sup>17, 21-22</sup> Recently, we have demonstrated that porous alumina overcoating on Pd catalyst can considerably enhance the selectivity to butenes.<sup>23</sup> Nevertheless, the improvement of 1-butene selectivity is still limited.

On atomically dispersed Pd atoms, the adsorption mode of 1,3-butadiene is expected to be a single carbon-carbon double bond involved mono- $\pi$ -adsorption, in sharp contrast with the one on Pd nanoparticle surface, thus it might provide a new opportunity to further improve the selectivity to butenes, especially to 1-butene. To confirm this idea, here we first fabricated a single-atom Pd catalyst on graphene using the ALD technique, because the type and amount of oxygen functional groups on carbon-based materials for anchoring the Pd ALD precursor, palladium hexafluoroacetylacetonate (Pd(hfac)<sub>2</sub>), can be carefully controlled to ensure that the selected anchor sites can not only react with Pd(hfac)<sub>2</sub>, but also immobilize the Pd atom after removal of the hfac ligands under the ALD conditions.<sup>24</sup> The dominant presence of isolated Pd atoms on graphene was confirmed by aberration-corrected high-angle annular dark-field scanning transmission electron microscopy (HAADF-STEM) and X-ray absorption fine structure spectroscopy (XAFS). Indeed, in selective hydrogenation of 1,3-butadiene, the resulted single-atom Pd<sub>1</sub>/graphene catalyst demonstrated superior catalytic

performance, by achieving 100% butenes selectivity, particularly the highest ever 1-butene selectivity of ~70% at 95% conversion at about 50 °C, and excellent durability during a total 100 h of reaction time on stream.

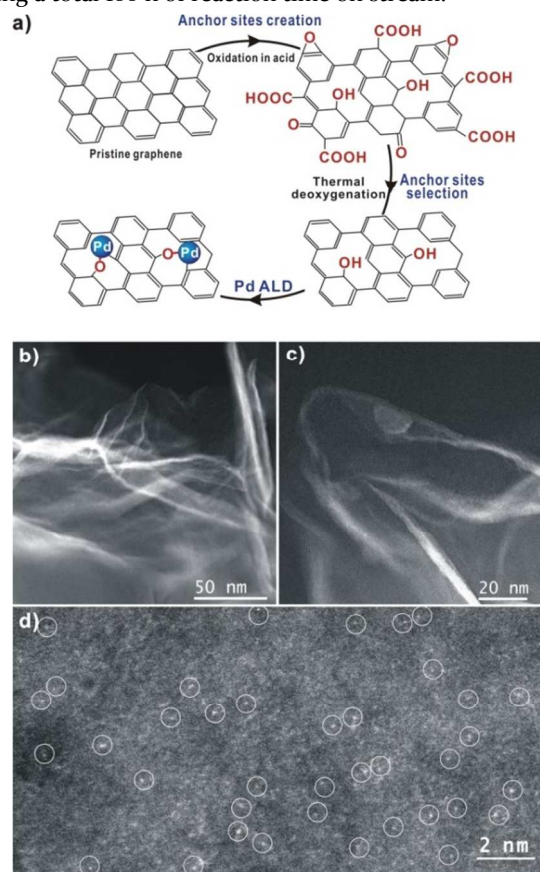


**Figure 1.** (a) A schematic illustration of single-atom Pd<sub>1</sub>/graphene catalyst synthesis via a process of anchor sites creation and selection and Pd ALD on pristine graphene. Representative HAADF-STEM images of Pd<sub>1</sub>/graphene at low (b-c) and high (d) magnifications. Atomically dispersed Pd atoms in image (d) are highlighted by the white circles.

Before Pd ALD, anchor sites creation on pristine graphene nanosheets was first carried out by oxidation using the procedure described previously (Figure 1a).<sup>25</sup> Then, the obtained graphene oxide powder was carefully reduced via thermal deoxygenation to precisely tune the type and amount of surface oxygen functional groups (anchor sites selection). After annealing at 1050 °C for about 2 min under helium, X-ray photoemission spectroscopy (XPS) measurements revealed that the dominated oxygen species remained on the graphene support were phenolic oxygen (O1s binding energy of 533.4 eV, Figures S1), consistent very well with the previous literature.<sup>24</sup> Next, Pd ALD was performed on the reduced graphene support to synthesize single-atom Pd catalyst by alternately exposing Pd(hfac)<sub>2</sub> and formalin at 150 °C.<sup>26-27</sup> Inductively coupled plasma-atomic emission spectroscopy (ICP-AES) showed that the Pd loading was 0.25wt% after performing one Pd ALD cycle (designated as Pd<sub>1</sub>/graphene, shown in Table S1). Compared with the naked graphene (Figure S2), HAADF-STEM illustrated that Pd clusters were barely present on Pd<sub>1</sub>/graphene at both low and high magnifications (Figures 1 and S3); meanwhile, it clearly shows that individual Pd atoms were randomly

dispersed on the graphene support.

However, when the graphene oxide powder was annealed at lower temperatures, the Pd loading was high (Table S1), and a considerable fraction of Pd nanoparticles along with atomically dispersed Pd atoms were observed by STEM (Figure S4, designated as Pd-NPs/graphene). On the other hand, annealing at 1050 °C for a longer time would cause a dramatic decrease in the amount of phenolic oxygen, and thus the Pd loading became neglectable (Table S1), which is undesired for practical applications. Taken together, we propose that isolated phenol groups are the active sites for anchoring the Pd(hfac)<sub>2</sub> precursor, by forming -O-Pd-hfac surface species and Hhfac gaseous product, similar to the reaction between Pd(hfac)<sub>2</sub> and hydroxyls on oxide surfaces;<sup>27</sup> next, isolated Pd single atoms are formed after removing the rest hfac ligand by formalin exposure.<sup>27</sup>

Figure 2a shows the X-ray absorption near-edge structure (XANES) spectra of Pd<sub>1</sub>/graphene, Pd-hfac/graphene and Pd-NPs/graphene, and the reference spectra of Pd(hfac)<sub>2</sub>, Pd foil, and PdO for comparison. The shape characteristic peaks **A** (24367 eV) and **B** (24390 eV) of Pd-NPs/graphene are similar to that of Pd foil, indicating the Pd atoms are in the zero-valence state. However, the XANES spectrum of Pd<sub>1</sub>/graphene is close to those of Pd(hfac)<sub>2</sub> and PdO, which implies that the isolated Pd atoms on graphene surface were mostly present in a +2 valence state.

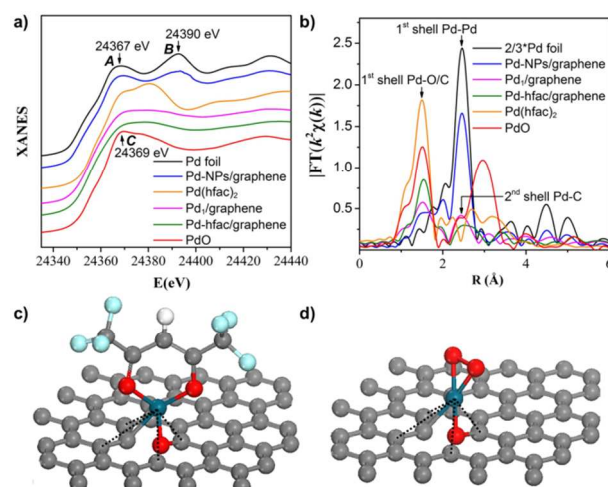


**Figure 2.** The XANES spectra at the Pd K-edge (a) and the K<sub>2</sub>-weighted Fourier transform spectra (b) of Pd<sub>1</sub>/graphene, Pd-NPs/graphene, Pd(hfac)<sub>2</sub>, PdO and Pd foil. Schematic models of (c) Pd-hfac/graphene and (d) Pd<sub>1</sub>/graphene, where the balls in gray, red, dark cyan, light blue and white represent carbon, oxygen, palladium, fluorine and hydrogen atoms, respectively. The Pd-C<sub>2</sub> coordination was indicated by the black dash line in (c-d).

More structural information could be provided by the measurements of extended x-ray absorption fine structure (EXAFS) at the Pd K-edge, as shown in Figure 2b. It can be found that the intensity of the first peak at about 1.6 Å for Pd<sub>1</sub>/graphene is significantly lower than that of PdO and Pd(hfac)<sub>2</sub>, implying a high distorted structure around the nearest coordination of Pd atoms. Moreover, the STEM images in Figures 1 and S3 revealed nearly all Pd are present as isolated atoms on graphene support. Hence, different from PdO and Pd(hfac)<sub>2</sub>, the first shell peak for Pd<sub>1</sub>/graphene is contributed to the mixture of Pd-O and Pd-C coordination: Pd-C<sub>1</sub> with the carbon atom from the graphene support, Pd-

O<sub>1</sub> with the oxygen atom bridging the Pd atom and the graphene support, and Pd-O<sub>2</sub> with the oxygen atoms on the side of away from graphene support, as shown in the model in Figure 2d. The bond lengths for Pd-C<sub>1</sub>, Pd-O<sub>1</sub>, and Pd-O<sub>2</sub> are 2.00 Å, 2.05 Å, and 2.07 Å, respectively (Table S2, the fitting curves can be found in Figures S5 and S6). Meanwhile, the second peak at about 2.5 Å for the Pd<sub>1</sub>/graphene is much weaker and similar to the Pd-hfac/graphene. The EXAFS analysis indicates that the second peak can be ascribed to the Pd-C<sub>2</sub> and Pd-Pd coordinations, where the carbon atoms are from the graphene support (Figure 2d) and Pd-Pd coordination is likely from the existence of Pd nanoclusters (Figures S7 and S8). However, the content of Pd nanoclusters is in a quite low level as revealed by the low Pd-Pd coordination number (Table S2) and STEM images (Figures 1 and S3); hence, they would not influence and contribute to the overall catalytic properties of the catalyst.

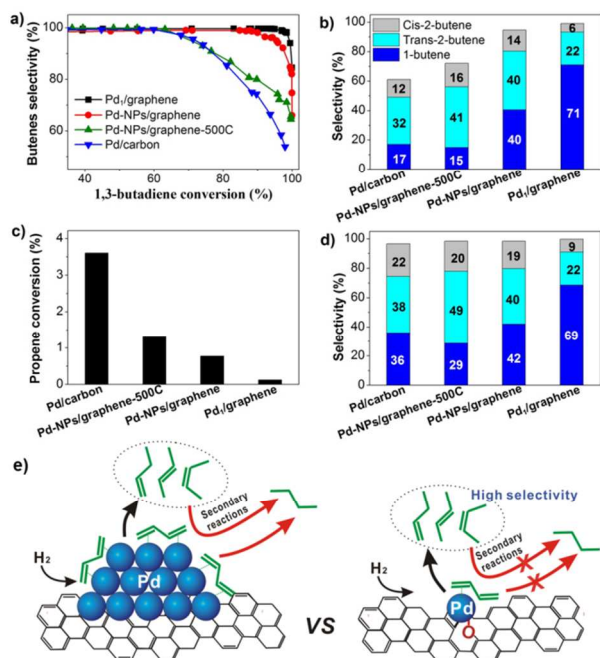


**Figure 3.** Catalytic performances of Pd<sub>1</sub>/graphene, Pd-NPs/graphene, Pd-NPs/graphene-500C, and Pd/carbon samples in selective hydrogenation of 1,3-butadiene. (a) Butenes selectivity as a function of conversion by changing the reaction temperatures; (b) the distribution of butenes at 95% conversion. Propene conversion (c) and the distribution of butenes (d) at 98% 1,3-butadiene conversion in hydrogenation of 1,3-butadiene in the presence of propene. (e) A schematic illustration of improvement of butenes selectivity on single-atom Pd<sub>1</sub>/graphene catalyst. Note: the figure legend in (b) also applies to (d).

Next, the catalytic performance of the single-atom Pd<sub>1</sub>/graphene catalyst was evaluated and compared to three different Pd nanoparticle catalysts in selective hydrogenation of 1,3-butadiene, as shown in Figures 3a and S9. On a commercial Pd/carbon catalyst (Figure S10), the selectivity to all butenes decreased dramatically when conversion was above 70%. Pd-NPs/graphene showed a better performance, retaining ~100% butenes selectivity up to 90% conversion. However, when it was annealed at 500 °C in Ar for 1 h (designated as Pd-NPs/graphene-500C, Figure S11) to largely reduce the contributions from the isolated Pd atoms

observed by STEM in Figure S4, the butenes selectivity started decreasing at a lower conversion of 70%, similar to Pd/carbon. Compared to these Pd nanoparticle catalysts, Pd<sub>1</sub>/graphene clearly demonstrated a superior catalytic performance by preserving 100% butenes selectivity up to 95% conversion, therein, the selectivity to 1-butene, the most desirable product, was nearly constant at as high as 71% (Figures 3b and S12), which is the highest ever value at such high conversion so far, seen in Table S3. Even under the practical conditions required for purification of industrial alkenes streams (adding 70% propene into the feed gas), Pd<sub>1</sub>/graphene again illustrated remarkably high catalytic performance by suppressing the propene conversion to only 0.1%, much more sufficiently than other catalysts (Figure 3c), and preserving high selectivity to butenes (100%) and especially to 1-butene (69%) at 98% conversion (Figure 3d).

The temperature effect on the butenes selectivity seems to be minor (Figures S13, S14, and Table S3). We speculate that butadiene adsorbs on the isolated Pd atoms very likely via the mono- $\pi$ -adsorption mode, rather than the di- $\pi$ -adsorption, since the later one usually requires a large ensemble of Pd surface (Figure 3e).<sup>28-29</sup> The mono- $\pi$ -adsorption mode disfavors simultaneously hydrogenating the two carbon-carbon double bonds of the butadiene molecule for butane formation, but encourages 1,2 hydrogen addition to form 1-butene, explaining the extraordinarily high 1-butene selectivity. Moreover, the Pd geometric effect induced higher packing density of butadiene on isolated Pd atoms than on Pd nanoparticles, will further enhance the steric effect, and thus more effectively inhibit the secondary hydrogenation reactions (Figure 3e). Nevertheless, the reaction mechanism, including the factors of the charging effect and the role of the Pd-carbon interaction<sup>30-31</sup> on the catalytic performance of Pd<sub>1</sub>/graphene remains to be further investigated. Meanwhile, we noticed that the TOF of Pd single atoms was 0.35 s<sup>-1</sup> at 47 °C, slightly lower than the two Pd nanoparticle catalysts measured in this work (Table S4). Therefore, Pd SAC provides another promising way to improve selectivity in hydrogenation reactions besides the conventional methods.<sup>17-20, 32-33</sup>

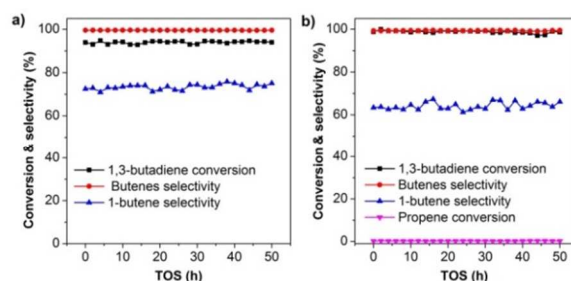


**Figure 4.** Durability test on Pd<sub>1</sub>/graphene first in the absence of propene for 50 h (a), and then in the presence of 70% propene for another 50 h (b) at about 50 °C.

The durability of Pd<sub>1</sub>/graphene was further tested first in the absence of propene for 50 h at 95% conversion, and then in the presence of an excess of propene for another 50 h at a conversion near 100%. As shown in Figure 4, Pd<sub>1</sub>/graphene showed excellent durability against deactivation during a total 100 h of reaction time on stream (TOS) without any visible activity decline or selectivity change (also seen in Figure S15). To the best of our knowledge, this is the best ever durability at near ambient temperatures among all the

metal catalysts reported in the literatures so far (Table S5). It is worthy to note that no any visible metal atom aggregation was observed by STEM on the spent catalyst after either a total 100 h of reaction time on stream (Figure S16), or annealing at 400 °C in Ar for 1 h (Figure S17).

In conclusion, we have successfully demonstrated that atomically dispersed Pd on graphene can be achieved using ALD by a careful control over the oxygen functional groups on the graphene surface. HAADF-STEM and XAFS both confirmed the dominant presence of isolated Pd atoms. When the single-atom Pd/graphene catalyst was evaluated in selective hydrogenation of 1,3-butadiene, it revealed superior catalytic performance, showing about 100% butenes selectivity, especially the highest ever 1-butene selectivity of ~70% at a conversion of 95% at a mild reaction condition of about 50 °C. In the presence of an excess of propene, the propene stream was greatly preserved by sufficiently suppressing its conversion to only 0.1%. We speculate that the mono- $\pi$ -adsorption mode of 1,3-butadiene and the enhanced steric effect induced by 1,3-butadiene adsorption on isolated Pd atoms both play important roles in the improvement of butenes selectivity. More importantly, Pd/graphene showed excellent durability against deactivation via either metal atom aggregation or coking during a total 100 h of reaction time on stream. Finally, our work suggests that SACs might open up new opportunities in selective hydrogenation reactions for improved selectivity and durability besides water-gas shift (WGS)<sup>3</sup> and oxidation reactions.<sup>1</sup>

## ASSOCIATED CONTENT

### Supporting Information

Experimental section, additional characterizations and catalytic performances tests. This information is available free of charge via the Internet at <http://pubs.acs.org>.

## AUTHOR INFORMATION

### Corresponding Author

junling@ustc.edu.cn  
sqwei@ustc.edu.cn

### Author Contributions

<sup>†</sup>These authors contributed equally.

### Notes

The authors declare no competing financial interests. Any additional relevant notes should be placed here.

## ACKNOWLEDGMENT

This work was supported by the One Thousand Young Talents Program under the Recruitment Program of Global Experts, the NSFC (21473169, 11135008, and 51402283), the Fundamental Research Funds for the Central Universities (WK2060030014), and the startup funds from University of Science and Technology of China.

## REFERENCES

(1) Yang, X. F.; Wang, A. Q.; Qiao, B. T.; Li, J.; Liu, J. Y.; Zhang, T., *Acc. Chem. Res.* **2013**, 46, 1740-1748.

- (2) Flytzani-Stephanopoulos, M.; Gates, B. C., *Annu Rev Chem Biomol* **2012**, 3, 545-574.
- (3) Flytzani-Stephanopoulos, M., *Acc. Chem. Res.* **2014**, 47, 783-792.
- (4) Qiao, B. T.; Wang, A. Q.; Yang, X. F.; Allard, L. F.; Jiang, Z.; Cui, Y. T.; Liu, J. Y.; Li, J.; Zhang, T., *Nat. Chem.* **2011**, 3, 634-641.
- (5) Yang, M.; Li, S.; Wang, Y.; Herron, J. A.; Xu, Y.; Allard, L. F.; Lee, S.; Huang, J.; Mavrikakis, M.; Flytzani-Stephanopoulos, M., *Science* **2014**, 346, 1498-1501.
- (6) Zhang, X.; Shi, H.; Xu, B. Q., *Angew. Chem. Int. Ed.* **2005**, 44, 7132-7135.
- (7) Kochubey, D. I.; Chesnokov, V. V.; Malykhin, S. E., *Carbon* **2012**, 50, 2782-2787.
- (8) Peterson, E. J.; Delariva, A. T.; Lin, S.; Johnson, R. S.; Guo, H.; Miller, J. T.; Kwak, J. H.; Peden, C. H. F.; Kiefer, B.; Allard, L. F.; Ribeiro, F. H.; Datye, A. K., *Nat. Commun.* **2014**, 5.
- (9) Corma, A.; Concepcion, P.; Boronat, M.; Sabater, M. J.; Navas, J.; Yacaman, M. J.; Larios, E.; Posadas, A.; Lopez-Quintela, M. A.; Buceta, D.; Mendoza, E.; Guilera, G.; Mayoral, A., *Nat. Chem.* **2013**, 5, 775-781.
- (10) Moses-DeBusk, M.; Yoon, M.; Allard, L. F.; Mullins, D. R.; Wu, Z. L.; Yang, X. F.; Veith, G.; Stocks, G. M.; Narula, C. K., *J. Am. Chem. Soc.* **2013**, 135, 12634-12645.
- (11) Sun, S. H.; Zhang, G. X.; Gauquelin, N.; Chen, N.; Zhou, J. G.; Yang, S. L.; Chen, W. F.; Meng, X. B.; Geng, D. S.; Banis, M. N.; Li, R. Y.; Ye, S. Y.; Knights, S.; Botton, G. A.; Sham, T. K.; Sun, X. L., *Sci. Rep.* **2013**, 3, 1775.
- (12) Lu, J. L.; Elam, J. W.; Stair, P. C., *Acc. Chem. Res.* **2013**, 46, 1806-1815.
- (13) Suntola, T.; Hyvarinen, J., *Annu. Rev. Mater. Sci.* **1985**, 15, 177-195.
- (14) Stambula, S.; Gauquelin, N.; Bugnet, M.; Gorantla, S.; Turner, S.; Sun, S. H.; Liu, J.; Zhang, G. X.; Sun, X. L.; Botton, G. A., *J. Phys. Chem. C* **2014**, 118, 3890-3900.
- (15) Derrien, M. L., *Stud. Surf. Sci. Catal.* **1986**, 27, 613-666.
- (16) Hugon, A.; Delannoy, L.; Louis, C., *Gold Bull.* **2008**, 41, 127-138.
- (17) Crabb, E. M.; Marshall, R., *Appl. Catal. a-Gen.* **2001**, 217, 41-53.
- (18) El Kolli, N.; Delannoy, L.; Louis, C., *J. Catal.* **2013**, 297, 79-92.
- (19) Sarkany, A.; Zsoldos, Z.; Stefler, G.; Hightower, J. W.; Gucci, L., *J. Catal.* **1995**, 157, 179-189.
- (20) Goetz, J.; Volpe, M. A.; Gigola, C. E.; Touroude, R., *J. Catal.* **2001**, 199, 338-345.
- (21) Cervantes, G. G.; Aires, F. J. C. S.; Bertolini, J. C., *J. Catal.* **2003**, 214, 26-32.
- (22) Ahn, I. Y.; Lee, J. H.; Kim, S. K.; Moon, S. H., *Appl. Catal. a-Gen.* **2009**, 360, 38-42.
- (23) Yi, H.; Du, H. Y.; Hu, Y. L.; Yan, H.; Jiang, H.-L.; Lu, J. L., *ACS Catal.* **2015**, 5, 2735-2739.
- (24) Ganguly, A.; Sharma, S.; Papakonstantinou, P.; Hamilton, J., *J. Phys. Chem. C* **2011**, 115, 17009-17019.
- (25) Hummers, W. S.; Offeman, R. E., *J. Am. Chem. Soc.* **1958**, 80, 1339-1339.
- (26) Lu, J.; Stair, P. C., *Langmuir* **2010**, 26, 16486-16495.
- (27) Elam, J. W.; Zinovev, A.; Han, C. Y.; Wang, H. H.; Welp, U.; Hryn, J. N.; Pellin, M. J., *Thin Solid Films* **2006**, 515, 1664-1673.
- (28) Goetz, J.; Volpe, M. A.; Touroude, R., *J. Catal.* **1996**, 164, 369-377.
- (29) Lee, D. C.; Kim, J. H.; Kim, W. J.; Kang, J. H.; Moon, S. H., *Appl. Catal. a-Gen.* **2003**, 244, 83-91.
- (30) Benavidez, A. D.; Burton, P. D.; Nogales, J. L.; Jenkins, A. R.; Ivanov, S. A.; Miller, J. T.; Karim, A. M.; Datye, A. K., *Appl. Catal. a-Gen.* **2014**, 482, 108-115.
- (31) Bauer, M.; Schoch, R.; Shao, L. D.; Zhang, B. S.; Knop-Gericke, A.; Willinger, M.; Schlögl, R.; Teschner, D., *J. Phys. Chem. C* **2012**, 116, 22375-22385.
- (32) Kyriakou, G.; Boucher, M. B.; Jewell, A. D.; Lewis, E. A.; Lawton, T. J.; Baber, A. E.; Tierney, H. L.; Flytzani-Stephanopoulos, M.; Sykes, E. C. H., *Science* **2012**, 335, 1209-1212.
- (33) Boucher, M. B.; Zugic, B.; Cladaras, G.; Kammert, J.; Marcinkowski, M. D.; Lawton, T. J.; Sykes, E. C. H.; Flytzani-Stephanopoulos, M., *Phys Chem Chem Phys* **2013**, 15, 12187-12196.

## Table of Contents Graphic

